THE JOURNAL OF BIOLOGICAL CHEMISTRY VOL. 291, NO. 14, pp. 7409–7417, April 1, 2016

A Method for Multiplexed Measurement of Mitochondrial Pyruvate Carrier Activity*

Received for publication, December 18, 2015, and in revised form, January 19, 2016 Published, JBC Papers in Press, January 28, 2016, DOI 10.1074/jbc.M115.711663

Lawrence R. Gray[1], **Adam J. Rauckhorst**[1], **and Eric B. Taylor**[2]

From the Department of Biochemistry, the Fraternal Order of the Eagles Diabetes Research Center, the Abboud Cardiovascular Research Center, and the Pappajohn Biomedical Institute, Carver College of Medicine, University of Iowa, Iowa City, Iowa 52242

The discovery that the *MPC1* and *MPC2* genes encode the protein components of the mitochondrial pyruvate carrier (MPC) has invigorated studies of mitochondrial pyruvate transport and its regulation in normal and disease states. Indeed, recent reports have demonstrated MPC involvement in the control of cell fate in cancer and gluconeogenesis in models of type 2 diabetes. Biochemical measurements of MPC activity are foundational for understanding the role of pyruvate transport in health and disease. We developed a 96-well scaled method of [^{14}C]pyruvate uptake that markedly decreases sample requirements and increases throughput relative to previous techniques. This method was applied to determine the mouse liver MPC K_m (28.0 ± 3.9 μM) and V_{max} (1.08 ± 0.05 nmol/min/mg), which have not previously been reported. K_m and V_{max} of the rat liver MPC were found to be 71.2 ± 17 μM and 1.42 ± 0.14 nmol/min/mg, respectively. Additionally, we performed parallel pyruvate uptake and oxidation experiments with the same biological samples and show differential results in response to fasting, demonstrating the continued importance of a direct MPC activity assay. We expect this method will be of value for understanding the contribution of the MPC activity to health and disease states where pyruvate metabolism is expected to play a prominent role.

Pyruvate is a central metabolite linking cytoplasmic and mitochondrial metabolism. In the cytosol, pyruvate is generated as the terminal product of glycolysis, from amino acid interconversions and transamination reactions, and from oxidation of lactate. After transport across the mitochondrial inner membrane, pyruvate is converted to acetyl-CoA or oxaloacetate through the respective activities of pyruvate dehydrogenase or pyruvate carboxylase. Acetyl-CoA provides carbon for the tricarboxylic acid cycle, whereas oxaloacetate may be shunted toward either the tricarboxylic acid cycle or gluconeogenesis, depending upon prevailing metabolic demands. The critical protein complex linking these cytosolic and mitochondrial processes is the mitochondrial pyruvate carrier (MPC),[3] which imports pyruvate across the mitochondrial inner membrane barrier into the matrix. Although a distinct, biochemically inhibitable MPC activity was identified over four decades ago, the genes encoding the MPC have only recently been identified (1, 2).

The MPC is an orphan carrier that is distantly related to the SemiSWEET family of bacterial transporters rather than the canonical *SLC25A* family of mitochondrial solute carriers (3, 4). The MPC complex comprises two paralogous subunits, MPC1 and MPC2. The stoichiometry of these subunits has yet to be determined but is potentially dynamic (5). MPC1 is ~12 kDa with two predicted transmembrane domains. MPC2 is slightly larger at 14 kDa and contains three predicted transmembrane domains (6). Loss of either MPC1 or MPC2 protein results in the destabilization and degradation of the other and thus loss of the MPC complex (7, 8).

More recent investigations have demonstrated that the MPC may be a point of altered metabolic regulation in disease states such as cancer, obesity, and type 2 diabetes (6–11). Hepatic *Mpc1* transcript and MPC1 and MPC2 protein levels are increased in the high fat diet-induced obesity mouse model of type 2 diabetes; this could contribute to increased gluconeogenic carbon flux (7, 8). In contrast, loss of MPC activity in models of cancer promotes a Warburg-like metabolism with increased glutamine utilization that could contribute to oncogenic transformation (9–11). The MPC proteins may also be covalently regulated by post-translational modifications. Mitochondrial proteome screens have identified several post-translational modifications to MPC1 and MPC2 in response to fasting and a high fat-fed mouse model of diabetes (12, 13). However, the effects of these modifications on MPC function have not been determined. Given the central metabolic node occupied by the MPC, changes in MPC activity, either through post-translational modifications or protein abundance, may profoundly regulate overall cellular metabolism.

Several methods have been developed to measure the MPC-specific activity. For each of these methods, mitochondria are incubated in a buffer containing radiolabeled pyruvate. Over time, the MPC transports pyruvate into the matrix until that assayed is stopped. Each method quantifies mitochondrial

* This work was supported by National Institutes of Health Grants R01 DK104998 (to E. B. T.), R00 AR059190 (to E. B. T.), F32 DK101183 (to L. R. G.), T32 HL007121 to Francois Abboud (to L. R. G.), T32 HL007638 to Michael Welsh (to A. J. R.), and P30CA086862 to George Weiner, which contributed to support of core facilities utilized for this work. The authors declare no conflict of interest. The content is solely the responsibility of the authors and does not necessarily represent the official views of the National Institutes of Health.

[1] Both authors contributed equally to this work.

[2] To whom correspondence should be addressed: Carver College of Medicine, University of Iowa, 169 Newton Rd., 3316 Pappajohn Biomedical Research Bldg., Iowa City, IA 52242. E-mail: eric-taylor@uiowa.edu.

[3] The abbreviations used are: MPC, mitochondrial pyruvate carrier; TMPD, *N*,*N*,*N*′,*N*′-tetramethyl-*p*-phenylenediamine dihydrochloride; MIB, mitochondrial isolation buffer; UB, uptake buffer; CHC, α-cyano-4-hydroxycinnamic acid; FCCP, carbonyl cyanide *p*-trifluoromethoxyphenylhydrazone.

matrix-localized radiolabeled pyruvate using a scintillation counter for calculation of a relative MPC specific activity. The chief difference among these methods is how mitochondrial pyruvate uptake is halted. Techniques that have been used for halting uptake include centrifugation to pellet the mitochondria (14, 15), filtration through a membrane to separate mitochondria and uptake buffer (16), and a rapid density gradient separation (17). However, the gold standard method is the inhibitor stop technique (15, 18), which utilizes specific MPC chemical inhibitors like UK5099 and α-cyano-4-hydroxycinnamic acid (CHC) to halt mitochondrial pyruvate uptake.

There are significant advantages of halting uptake using the inhibitor stop approach. Inhibitors terminate uptake on a much faster time scale compared with centrifugation or filtration techniques, allowing for resolved capture of kinetic information. In addition, the use of inhibitors in wash buffers after stopping uptake prevents export of matrix pyruvate. However, despite these technical strengths of the inhibitor stop method, it has been labor- and sample-intensive. Milligram amounts of mitochondria per time point have been required. Previous kinetic studies have been applied to model systems such as rat liver where large amounts of mitochondria are easily obtained (18). With the prevalence of transgenic mouse models and cell culture systems where raw material is more limited, a more efficient method is required for practical measurements of MPC activity.

We report the development of a 96-well scaled mitochondrial pyruvate uptake assay for multiplexed measurement of the MPC specific activity. Our method requires decreased amounts of mitochondrial sample and markedly decreased assay time per sample and greatly increases overall throughput. We demonstrate the utility of this method by determining the kinetics of the mouse liver MPC specific activity.

Experimental Procedures

Animal Care—All animal experiments were conducted in accordance with the University of Iowa Animal Use and Care Committee. Mouse experiments were performed with 11–14-week-old C57 Bl6/J male mice purchased from The Jackson Laboratory (catalog number 000664). Rat experiments were performed with Sprague-Dewey rats purchased at a weight of 275–300 g from Harlan Laboratories (catalog number 211M).

Buffers—The following buffers were used in this protocol. Mitochondrial isolation buffer (MIB) contained 70 mM sucrose, 210 mM D-mannitol, 5 mM HEPES, pH 7.4, 1 mM EGTA, and 0.5% fatty acid-free bovine serum albumin (Sigma, catalog number A3803). Uptake buffer (UB) contained 120 mM KCl, 5 mM HEPES, pH 7.4, 1 mM EGTA, 2 μM rotenone, and 2 μM antimycin A. 2× PYR buffer contained 120 mM KCl, 5 mM HEPES, pH 6.1, 1 mM EGTA, 2 μM rotenone, 2 μM antimycin A, and 0.0020–0.4000 mM [2-^{14}C]pyruvate as noted. Stop buffer contained 108 mM KCl, 4.5 mM HEPES, pH 6.8, 0.9 mM EGTA, 1.8 μM rotenone, 1.8 μM antimycin A, and 10 mM CHC (Sigma, catalog number 476870) (nine parts UB, pH 6.8, and one part 100 mM CHC). Wash buffer contained uptake buffer, pH 6.8, supplemented with 2 mM CHC and 10 mM pyruvate. Clark buffer contained 70 mM sucrose, 210 mM D-mannitol, 10 mM KH_2PO_4, 5 mM $MgCl_2$, 5 mM HEPES, pH 7.4, 1 mM EGTA, 0.2% fatty acid-free BSA, 5 mM succinate, pH 7.4, and 2 μM rotenone. Mitochondrial Seahorse buffer contained 70 mM sucrose, 210 mM D-mannitol, 10 mM KH_2PO_4, 5 mM $MgCl_2$, 5 mM HEPES, pH 7.4, 1 mM EGTA, and 0.2% fatty acid-free BSA.

Mitochondrial Isolation—Mitochondria were isolated as described previously by Rogers *et al.* (19) and as summarized in Fig. 1. Mice and rats were anesthetized by isoflurane inhalation and sacrificed via cervical dislocation or thoracotomy, respectively. Each liver was washed first in ice-cold PBS and second in ice-cold MIB. Livers, ~1.0 g (mouse) or ~13.0 g (rat) of wet tissue, were finely minced in 10 volumes of fresh MIB and homogenized in four passes of a motor rotated at 400–500 rpm using a Teflon-on-glass homogenizer. The homogenate was transferred to 50-ml tubes and centrifuged at 800 × *g* for 10 min at 4 °C (800 × *g* spin). The pellet was discarded, and the 800 × *g* supernatant was transferred to a polycarbonate tube and centrifuged at 8000 × *g* for 10 min (8000 × *g* spin). The 8000 × *g* pellet was resuspended in a similar volume of fresh MIB. If pyruvate oxidation assays were conducted in parallel, 2–3 × 0.3-ml aliquots of resuspended mitochondria were placed into 1.5-ml tubes and centrifuged at 9000 × *g* for 10 min at 4 °C. The supernatant was removed, and the pellet was kept on ice until resuspension and dispersal into assay vessels. For measuring mitochondrial pyruvate uptake, the remaining resuspended 8000 × *g* pellet was centrifuged at 9000 × *g* for 10 min at 4 °C. The 9000 × *g* pellet was resuspended in 1.10 ml of MIB and split into 1.0- and 0.1-ml aliquots in 1.5-ml tubes. These tubes were centrifuged at 9000 × *g* for 10 min at 4 °C. The supernatant was removed, and the pellets were kept on ice. The 0.10-ml pellet was diluted into 300 μl of PBS and used for Bradford assays (20) using the Bio-Rad Protein Assay Dye Reagent (catalog number 500-0006) prior to uptake assays to guide dilution of the 1.0-ml pellet for mitochondrial pyruvate uptake assays.

Multiplexed Mitochondrial Pyruvate Uptake—Mitochondria for measuring uptake were kept as pellets on ice until analysis. Mitochondria were resuspended to ~15.0 mg/ml in UB. The mitochondria were split into two equal volumes, one of which was treated with the MPC inhibitor CHC to a final concentration of 2 mM as a negative control and the other remaining in an equal volume of untreated UB. The mitochondria were incubated on ice for 5 min. Typically, each mitochondrial preparation was assayed for pyruvate uptake in quadruple technical replicates. Therefore, ~80 μl each of untreated and CHC-pretreated mitochondria were placed into 8 wells of a standard 96-well plate, alternating treatment conditions. To start the pyruvate uptake assay, an equal volume of mitochondria (65 μl) was added and mixed with an equal volume of 2× PYR buffer. This mixing of the UB mitochondrial preparations with the 2× PYR buffer yielded a final buffer with a pH of 6.8. Samples were taken at 5, 10, 20, and 30 s after the start of the assay. For each time point, to stop the assay, 30 μl of the uptake reaction was withdrawn from the reaction well and mixed with 70 μl of stop buffer in another well. After stopping the reaction, the mitochondria were separated from the reaction mixture using a 96-well vacuum manifold (Whatman Manifold I Spot Blot, catalog number 10447850). Efficiency of the assay is improved when two individuals work together with one person preparing the blot apparatus (see below) and performing the assay and the

second person trimming and processing the filters for data collection.

Vacuum Manifold Setup—Prior to the assay, manifold wells not to be used were sealed using 96-well plate sealers on both the top and bottom of the filter support plate as shown in Fig. 2*A*. For setup, the manifold was oriented with the filter support plate being placed upon the vacuum plenum with the vacuum line adapter facing toward the back. First, a piece of chromatography paper trimmed to ~4 × 3 inches (Whatman, catalog number 3030-6461) was wetted in wash buffer and placed atop the filter support. Second, a piece of plastic or Parafilm was placed over the top of the filters. This piece was cut like the plate sealers so that the inactive wells were blocked whereas the active wells were unobstructed. Third, a one-piece layer of 0.45-μm nitrocellulose membrane, also prewetted in wash buffer, was added. Fourth, a piece of 0.80-μm mixed cellulose ester filter (MF-Millipore, catalog number AAWP14250 or AAWP09000) was placed atop the 0.45-μm nitrocellulose membrane. A finger was run across the filters to eliminate air bubbles. Fifth, the sample well plate of the manifold apparatus was placed on top, and the manifold was clamped shut. Finally, Parafilm was stretched and wrapped around the entire apparatus in at least two layers as an extra safeguard against inward air leaks (see Fig. 2*B*). The layering of membranes, filters, and manifold is illustrated in Fig. 2*C*. The final prepared apparatus was connected to a vacuum source and placed ~⅔ deep into wetted iced. Prior to assays, to confirm the patency of the seal and ensure all wells drained correctly, 100 μl of water or wash buffer was passed through each well with the vacuum. If any well did not drain correctly, the entire apparatus was disassembled and prepared again. The underlying chromatography filter paper was replaced after each assay.

Multiplexed Washing and Separation of Postassay Mitochondria—With the vacuum on (~15 p.s.i.) and connected to the manifold apparatus assembled as described in the foregoing section and using a multichannel pipette, reaction mixtures from the 96-well plate (as shown in Fig. 2*D*) were transferred to the manifold. After every well in a row had drained, 200 μl of wash buffer was added and allowed to drain. This wash step was performed two to three times and results in mitochondria in each well being deposited on the ester layer in small discs. After all of the wells had drained, the manifold was removed from the vacuum line, and the Parafilm was removed. From this point in the assay, the ester and nitrocellulose filter layers were treated as a single layer as illustrated in Fig. 2*E*. This dual filter layer was cut into small squares for each mitochondrial disc as illustrated in Fig. 2*F*. Each sample was then individually placed into 7-ml plastic scintillation vials. Although a scalpel and tweezers can be used to handle and cut the filters, we highly recommend cutting the filters with a rotary cutter on a cutting mat, which can be obtained from a quilt or craft store. The cutting mat provides enough traction to keep the filters from moving during cutting and guide lines for consistent cutting. The rotary cutter allows for a safer and faster cut compared with the use of a scalpel. Finally, a 1- or 5-ml syringe with a 0.5-inch 27-gauge needle and a soft touch can be used as a tool to pick up and transfer the small membrane pieces into the scintillation vials. 5.5 ml of scintillation fluid (RPI Corp., BioSafe II, catalog number 111195) was added to the vials, which were capped and vortexed. Counts per minute were measured using a Beckman Coulter LS6500 scintillation counter.

Clark Electrode Studies—Oxygen consumption was determined using a Clark-type electrode. In brief, mitochondria were diluted to 0.5 mg/ml into Clark buffer. Once a basal respiration rate was achieved, rates of State III and State IV + oligomycin respiration were determined after the addition ADP to a final concentration of 100 μM and the successive addition of 1 μM oligomycin, respectively. Next, 0.2 μM FCCP was added to induce an uncoupled rate of oxygen consumption. Finally, 1 μM antimycin A was added to prevent electron transfer at Complex III and eliminate succinate-driven respiration. Each addition was made once a constant rate of respiration was achieved. The respiratory control ratio was determined as the State III rate/State IV + oligomycin rate.

High Resolution Respirometry Measurements—Pyruvate oxidation respirometry experiments were carried out essentially as described previously (19). A Seahorse Bioscience XF96 extracellular flux analyzer was used for all experiments. Briefly, aliquots of mitochondria were resuspended in 100 μl of mitochondrial Seahorse buffer. Mitochondrial protein concentration was measured using the Bio-Rad Protein Assay Dye Reagent, and samples were diluted to 0.25 mg/ml in mitochondrial Seahorse buffer. 20 μl of diluted mitochondria, for 5 μg of total mitochondrial protein, was loaded into V3-PET Seahorse plates and centrifuged at 2000 × *g* for 20 min. 160 μl of mitochondrial Seahorse buffer with 2.81 mM pyruvate + 0.28 mM malate was added to each well such that the final substrate concentration was 2.5 mM pyruvate + 0.25 mM malate. A three-injection protocol was performed. Triplicate measurements were performed after each injection, and each measurement consisted of a 1-min mixing step, a 1-min wait step, and a 3-min measurement step. First, basal oxygen consumption was measured. Second, oxygen consumption was stimulated with a combination of 4 mM ADP and 1 μM FCCP. Third, MPC specific activity was inhibited by 1 mM CHC. Finally, Complex I activity was inhibited by 1 μM rotenone.

Western Blotting—Standard Western blotting and SDS-PAGE methods were used. Briefly, samples were separated using either a 10 or 20% separating gel with a 4% stacking gel for 20 min at 100 V followed by 60 min at 200 V. Proteins were transferred to 0.2-μm nitrocellulose membrane (Amersham Biosciences, Protran, catalog number 10600001) at 100 V for 60 min. Blots were blocked for 1 h with 5% milk in TBS and incubated in primary antibody in 5% milk in TBS-Tween 20 overnight. Antibodies were used at the following concentrations: anti-VDAC, 1:1000 (Cell Signaling Technology, catalog number 4661S); anti-calreticulin, 1:1000 (Cell Signaling Technology, catalog number 2891S); anti-HSP90, 1:1000 (Cell Signaling Technology, catalog number 4874S); anti-pyruvate dehydrogenase, 1:1000 (Cell Signaling Technology, catalog number 3205S); and anti-MPC1, 1:1000 (a generous gift from Dr. Brian Finck). Blots were visualized using a LI-COR Odyssey CLx imager and a goat anti-rabbit DyLight 800 secondary antibody (1:5000; Thermo, catalog number SA5-35571).

Data Analysis and Statistics—The MPC specific activity was defined as activity of the non-CHC-treated samples less the

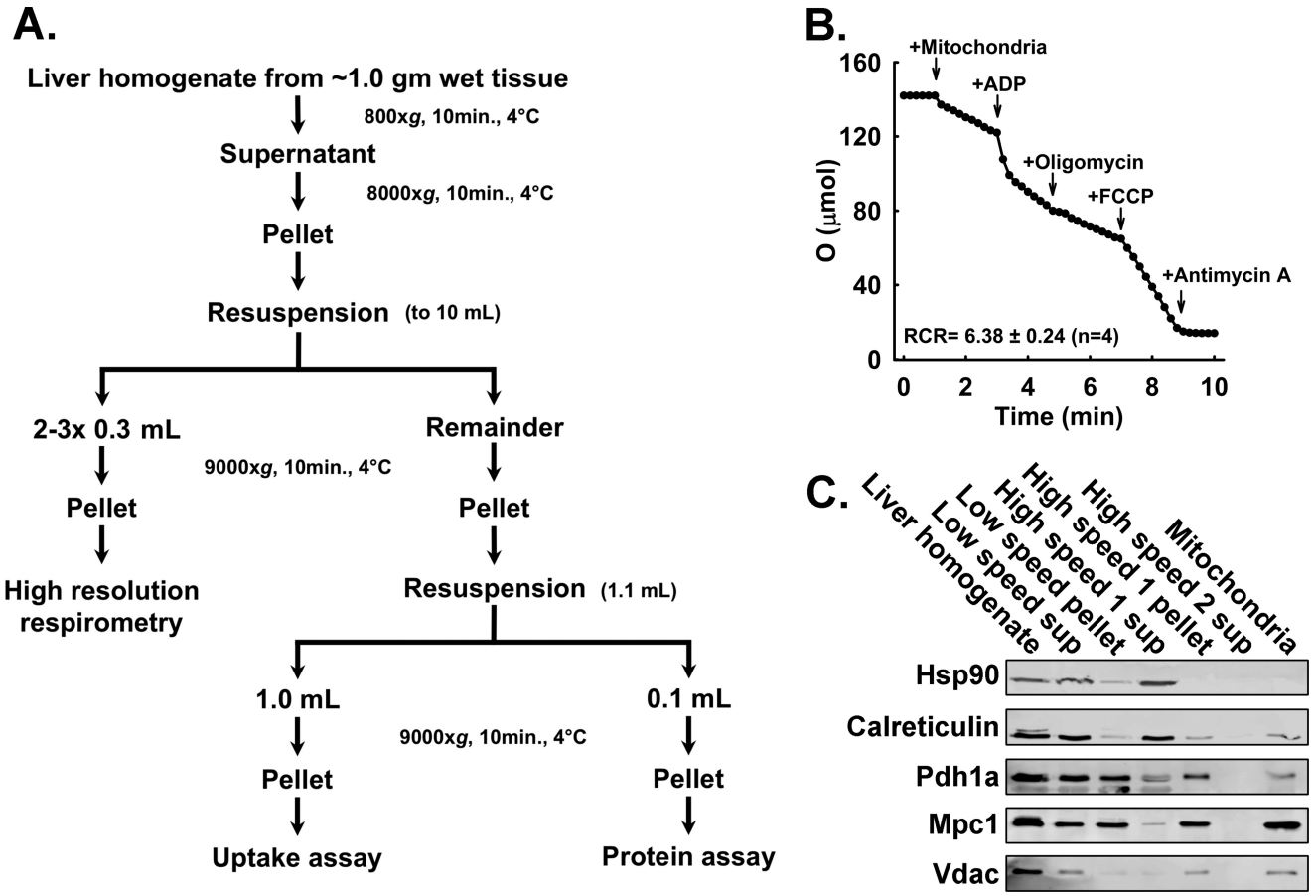

FIGURE 1. **Mitochondrial isolation and assessment of mitochondrial quality.** *A*, flow chart illustrating the mitochondrial isolation procedure including branch points for separating mitochondria for oxygen consumption by Seahorse extracellular flux analyzer and pyruvate uptake determination. *B*, representative trace acquired by a Clark-type electrode monitoring oxygen consumption of isolated mitochondria. The respiratory control ratio (State III rate/State IV + oligomycin rate) is shown ($n = 4$). *C*, Western blotting analysis of samples taken throughout the isolation procedure showing the purification of mitochondrial proteins (Hsp90, cytosolic marker; calreticulin, endoplasmic reticulum marker; Pdh1a, mitochondrial matrix marker; Mpc1, inner mitochondrial membrane; Vdac, mitochondrial inner membrane marker). *Sup*, supernatant.

activity of the CHC-treated samples (18). Specific activity relative to CPM was determined for each experiment by counting 10 μl of 2× PYR buffer and thus a known quantity of [^{14}C]pyruvate in triplicate in parallel with experimental samples.

Linear fits (Lineweaver-Burke) and one-site saturation fits (Michaelis-Menten) were performed in SigmaPlot. Initial rates were calculated using a linear fit with either SigmaPlot or Microsoft Excel. Figures were prepared using Microsoft PowerPoint and SigmaPlot. Data were organized in Microsoft Excel, and statistical outliers were identified using the Grubbs' test. Unless otherwise noted, data are represented as mean ± S.E.

Results

Our overall objectives were, first, to develop a method for measuring the MPC specific activity that enabled greater throughput with decreased sample requirements and, second, to test the efficacy of that method by determining the kinetics of the mouse liver mitochondrial MPC specific activity, which have not been reported previously. For these studies, intact, well coupled mouse liver mitochondria were required. We utilized a differential centrifugation protocol and buffers adapted from Rogers *et al.* (19) with the procedure summarized in Fig. 1*A*. Two quality control experiments were performed. First, succinate-driven respiration was measured using a Clark electrode. The resulting respiratory control ratio of 6.38 ± 0.24 (as shown in Fig. 1*B*) indicated that the isolated mitochondria robustly respire and were well coupled (21). Second, Western blotting analysis was performed on samples taken throughout the mitochondrial isolation procedure to gauge the overall purity of the mitochondrial isolations. The blots (shown in Fig. 1*C*) indicate that the final preparations were cytoplasm-free as shown by the marker HSP90 and contain only limited endoplasmic reticulum contamination as shown by the marker calreticulin (21, 22).

We reasoned that scaling the assay to a 96-well, multichannel pipette-compatible format and coupling the mitochondrial pyruvate uptake step to a 96-well vacuum manifold apparatus for washing and collecting postassay mitochondrial samples would simultaneously increase throughput while decreasing sample requirements. The use of the manifold, with required modifications in setup, is described in detail under "Experimental Procedures" and illustrated in Fig. 2. Primary considerations for manifold setup included prevention of vacuum leaks, effective washing and retention of mitochondrial samples, and an end point physical state of samples allowing easy transfer to scintillation vials for measuring ^{14}C content. Wells not to be

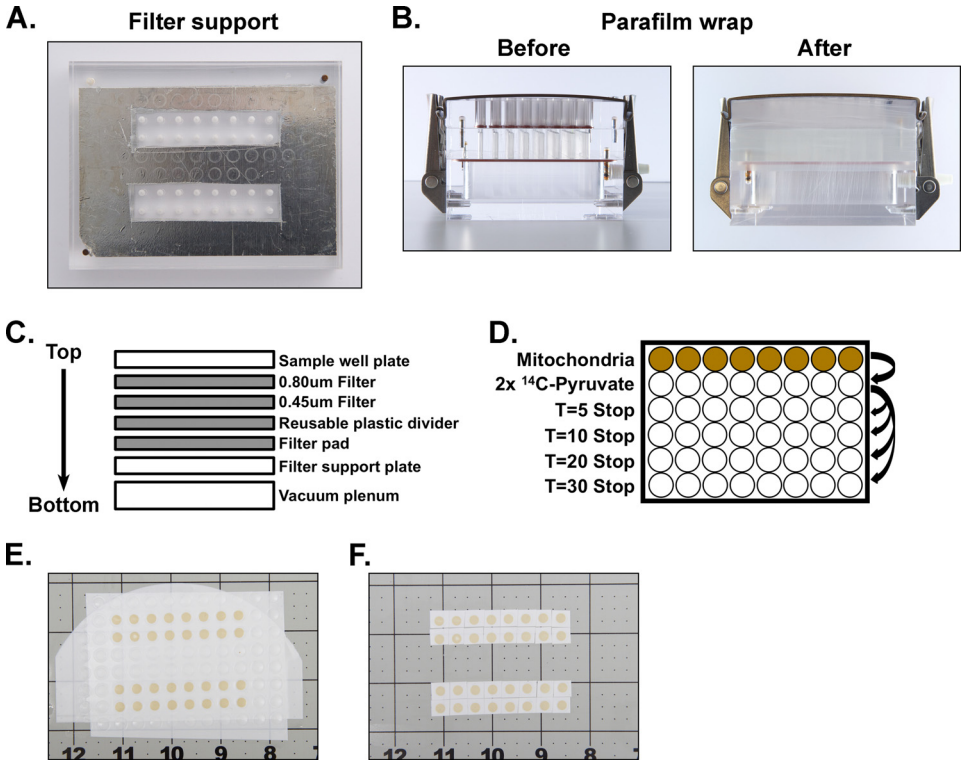

FIGURE 2. **Blot apparatus modification and setup.** *A*, modification of the filter support plate using 96-well plate covers to block non-utilized wells. *B*, fully assembled apparatus before and after Parafilm wrap. *C*, graphical representation of the assembled apparatus showing the layered order of filters within the completed assembly. *D*, graphical representation of a time course layout. *E*, filters containing mitochondrial samples after vacuum separation and washing steps prior to further processing. *F*, trimmed filter is removed, and mitochondrial samples are separated for [^{14}C]pyruvate analysis.

used for a particular assay were blocked using 96-well plate sealers as shown in Fig. 2*A*. The sealers can be easily removed and modified as needed to accommodate different and unique assay designs. An additional safeguard against leaks was implemented by tightly wrapping the outside of the assembled apparatus with Parafilm as shown in Fig. 2*B*.

To enable washing and retention of mitochondrial samples, we utilized a two-layer filter system with an upper layer of cellulose ester with 0.80-μm pores and an underlying layer of nitrocellulose with 0.45-μm pores. The larger pore size of the upper layer prevents clogging, and the smaller pore size of the lower layer prevents loss of minimal amounts of mitochondrial sample that pass through the upper layer. Because the washing step results in deposition of a mitochondrial disc on the filter layer, the final samples need not be perturbed prior to scintillation counting. Instead, the filter layer is cut into pieces for each mitochondrial disc as described under "Experimental Procedures" and used as a vehicle for transferring samples into scintillation vials for counting as shown in Fig. 2, *E* and *F*. Finally, the adjustable plate clamps were set to provide uniform pressure across the entire apparatus when closed. As an example of use, a typical time course experiment consists of 32 measurements with samples loaded in the middle of rows B, C, F, and G and loaded symmetrically across the apparatus to ensure uniform processing as shown in Fig. 2, *A* and *E*.

To test the efficacy of our method, mouse liver mitochondria were isolated, and a time course of the MPC specific activity was measured with pyruvate concentrations ranging from 0.001 to 0.200 mM. The collected data were used to calculate the MPC V_{max} and K_m of mouse liver mitochondria. The apparent linear phase of uptake is limited by a finite mitochondrial matrix volume. We observed that the uptake rate was near linear through 5–10 s with a rapid decrease in rate through 30 s, and our representative traces are shown in Fig. 3*A*. The initial rates through 5 s were determined and plotted against pyruvate concentration. The data were fitted to the Michaelis-Menten equation for determination of K_m and V_{max} values. The calculated K_m and V_{max} values for the mouse liver MPC specific activity were 28.0 $\pm$ 3.9 μM and 1.08 $\pm$ 0.05 nmol/min/mg of mitochondrial protein, respectively, as shown in Fig. 3, *B* and *C*. We also measured the kinetic properties of the MPC from rat liver mitochondria. We observed that the initial linear phase of pyruvate uptake was extended compared with mouse liver mitochondria, and therefore initial rates were calculated through 10 s (see Fig. 4*A*). The MPC from rat liver mitochondria manifested a K_m of 71.2 $\pm$ 17 μM and V_{max} of 1.42 $\pm$ 0.14 nmol/min/mg of mitochondrial protein as shown in Fig. 4, *B* and *C*.

Our observation that isolated mouse liver mitochondria display rapid uptake rates led us to investigate potential ways to extend the linear range of the assay. To increase the length of the initial linear phase of uptake, we pretreated mitochondria with a nanomolar amount of the potassium ionophore valinomycin (see Fig. 5*A*). Potassium transported by valinomycin at this concentration (3 nM) results in matrix swelling without rupturing the outer mitochondrial membrane (23). Although the linear range for the assay was increased, allowing for the calculation of initial rates through 10 s, valinomy-

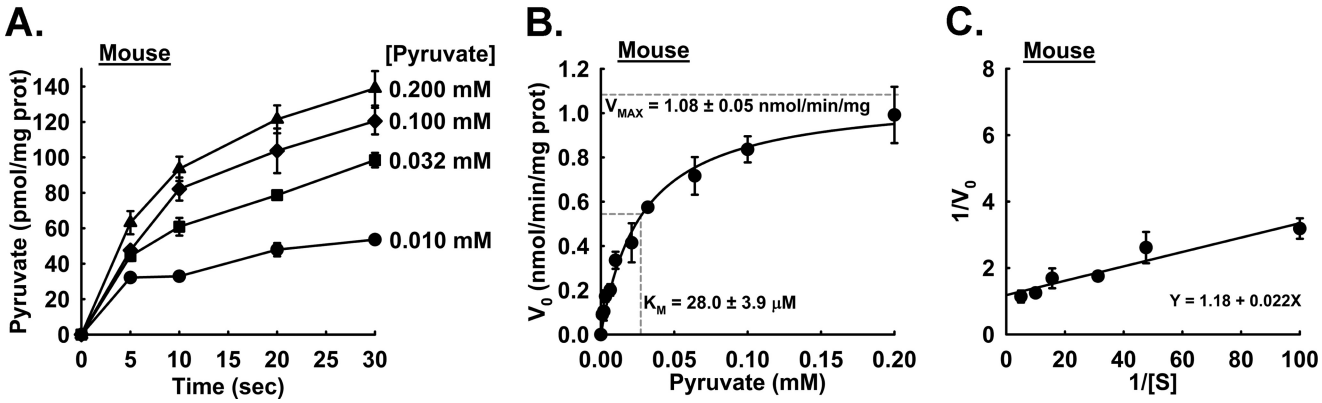

FIGURE 3. **Mitochondrial uptake and kinetics in isolated mouse liver mitochondria.** *A*, uptake of varying concentrations of pyruvate was monitored at the indicated time points in isolated mouse liver mitochondria ($n = 2–6$). Final pyruvate concentrations were: ●, 0.010 mM pyruvate; ■, 0.032 mM pyruvate; ◆, 0.100 mM pyruvate; ▲, 0.200 mM pyruvate. *B*, initial rates of pyruvate uptake in mouse liver mitochondria ($n = 3–10$ per concentration). $K_m = 28.0 \pm 3.9$ μM; $V_{max} = 1.08 \pm 0.05$ nmol/min/mg. *Horizontal dotted gray lines* represent the intersection of V_{max} and $^1/_2V_{max}$, and the *vertical dotted gray line* represents the K_m intersection. *C*, Lineweaver-Burk plot of rates shown in *A*. *Error bars* represent S.E. *prot*, protein.

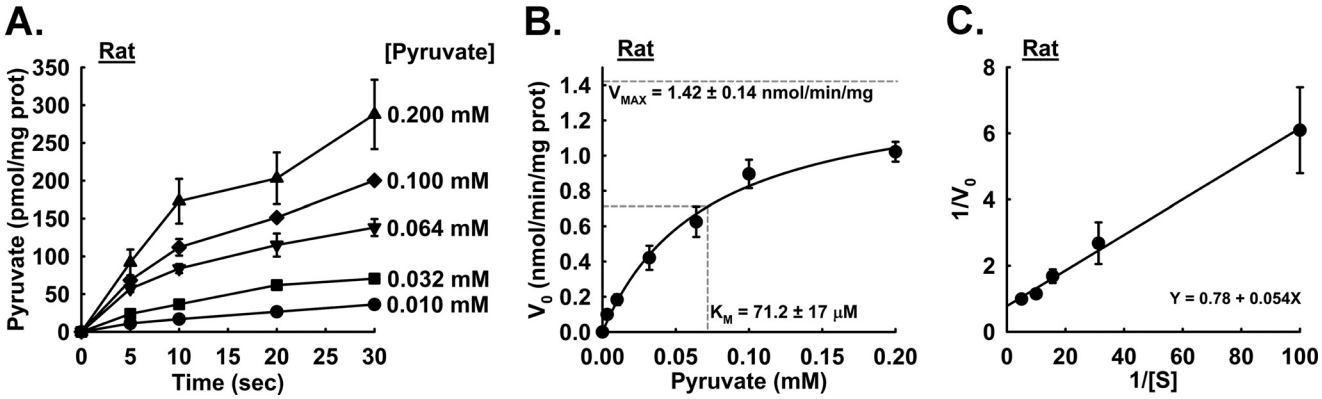

FIGURE 4. **Mitochondrial uptake and kinetics in isolated rat liver mitochondria.** *A*, uptake of varying concentrations of pyruvate was monitored at the indicated time points in isolated rat liver mitochondria ($n = 2–6$). Final pyruvate concentrations were: ●, 0.010 mM pyruvate; ■, 0.032 mM pyruvate; ▼, 0.064 mM pyruvate; ◆, 0.100 mM pyruvate; ▲, 0.200 mM pyruvate. *B*, initial rates of pyruvate uptake in rat liver mitochondria. $K_m = 71.2 \pm 17$ μM; $V_{max} = 1.42 \pm 0.14$ nmol/min/mg. *Horizontal dotted gray lines* represent the intersection of V_{max} and $^1/_2V_{max}$, and the *vertical dotted gray line* represents the K_m intersection ($n = 4$). *C*, Lineweaver-Burk plot of rates shown in *A*. *Error bars* represent S.E. *prot*, protein.

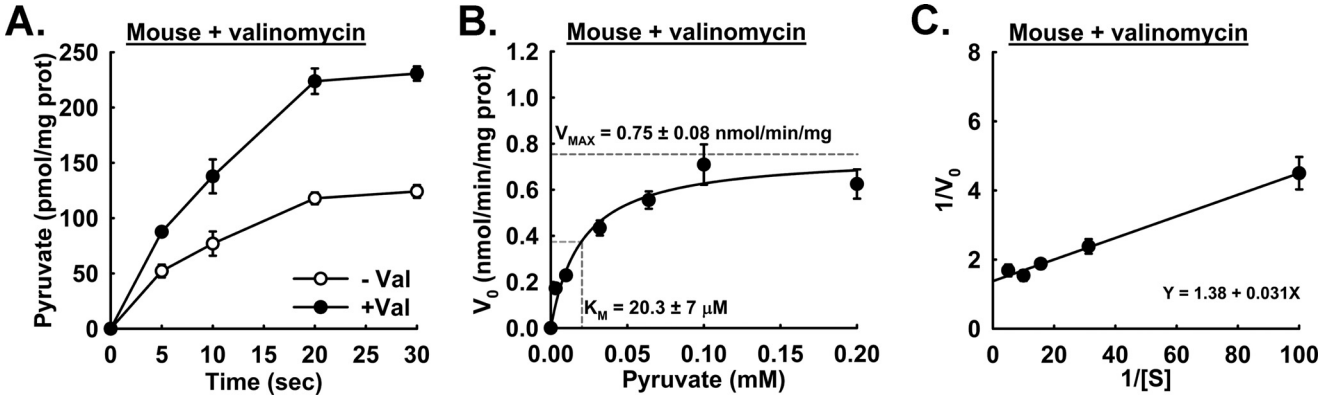

FIGURE 5. **Effects of pretreatment with valinomycin on initial linearity of pyruvate uptake in mouse liver mitochondria.** *A*, pyruvate uptake in mitochondria pretreated with (●; *solid circles*) or without (○; *open circles*) 3 nM valinomycin. Pyruvate concentration was 0.100 mM. *B*, initial rates of pyruvate uptake in mouse liver mitochondria pretreated with (●; *solid circles*) or without (○; *open circles*) 3 nM valinomycin. $K_m = 20.3 \pm 7$ μM; $V_{max} = 0.75 \pm 0.08$ nmol/min/mg. *Horizontal dotted gray lines* represent the intersection of V_{max} and $^1/_2V_{max}$, and the *vertical dotted gray line* represents the K_m intersection. *C*, Lineweaver-Burk plot of rates shown in *A*. *Error bars* represent S.E. *prot*, protein.

cin did not statistically change the K_m of mouse liver MPC (see Fig. 5, *B* and *C*).

To enable efficient use of biological samples, we designed our mitochondrial pyruvate uptake assay to be compatible with sample partitioning for parallel measurements of pyruvate oxidation. During the mitochondrial isolation, small fractions may be centrifuged separately for measurements of additional mitochondrial parameters as represented in Fig. 1*A*. For example, whereas the majority of mitochondria are required for the uptake assay, aliquots can be taken for other measures of mito-

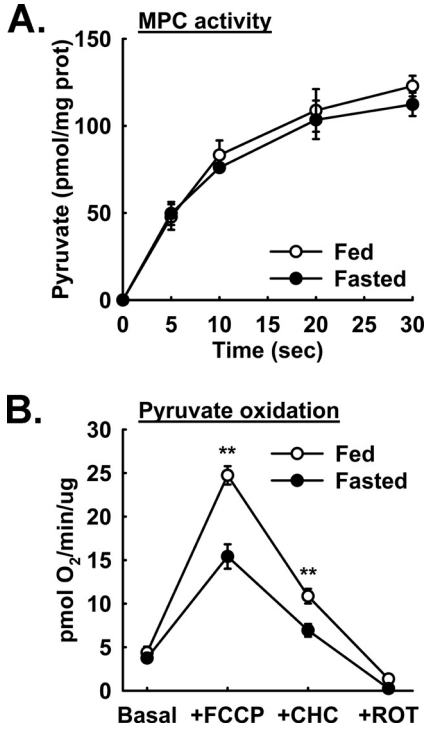

FIGURE 6. **Fasting induced changes in pyruvate oxidation but not pyruvate uptake.** *A*, pyruvate uptake by mouse liver mitochondria isolated from *ad libitum* fed (○; *open circles*) and 18-h fasted (●; *solid circles*) mice ($n = 4$). *B*, pyruvate-driven (2.5 mM pyruvate and 0.25 mM malate) respiration by mouse liver mitochondria isolated from *ad libitum* fed (○; *open circles*) and 18-h fasted (●; *solid circles*) mice ($n = 4$). *ROT*, rotenone; *prot*, protein. **, $p < 0.01$. *Error bars* represent S.E.

chondrial activity such as pyruvate oxidation using the Seahorse Bioscience XF96 analyzer or oxygen consumption experiments using a Clark electrode.

Previous reports have indicated changes in apparent MPC activity under certain physiological states such as diet-induced obesity (7, 8). We utilized our assay to test whether the liver MPC activity and rates of isolated liver mitochondrial pyruvate oxidation are altered by 18-h fasting in mice. No difference between fed and fasted mice was observed in pyruvate uptake (see Fig. 6*A*). Interestingly, mitochondria isolated from fasted animals displayed a significantly decreased oxygen consumption rate under FCCP/ADP-stimulated and, to a lesser extent, under CHC-treated conditions when pyruvate is used as a fuel source (see Fig. 6*B*). These results suggest that, although the MPC specific activity is not stably regulated by fasting, other stable intramitochondrial mechanisms spare pyruvate from oxidation presumably so that sufficient pyruvate is available for gluconeogenesis. Because the same initial mitochondrial sample was utilized to measure both pyruvate uptake and pyruvate oxidation, results can be more confidently compared than if samples had been obtained from separate samples.

Discussion

The recent discovery of the genes encoding the MPC (1, 2) has invigorated studies on the role of mitochondrial pyruvate transport and metabolism in health and disease. To facilitate these studies, we developed a mitochondrial pyruvate uptake assay with minimal sample requirements. The use of a 96-well vacuum blot apparatus allows for rapid and multiplexed analysis of radiolabeled pyruvate uptake in isolated mitochondria. The increased throughput of a multiwell system allows for the parallel analysis of replicates, either biological or technical, and therefore greater uniformity in sample processing and more confident quantitative analysis. This technique allows for pyruvate uptake to be determined in multiple unique mitochondrial preparations over the course of a few hours.

Previous determinations of MPC kinetics have been pursued in diverse model systems including mitochondria isolated from rat liver, rat heart muscle, and cultured cells. To compare our MPC kinetic data with previously obtained data, we performed a survey of the published MPC K_m and V_{max} values across multiple species and uptake methods, which are compiled in Table 1. MPC activity requires a proton-motive force because pyruvate import through the MPC requires co-proton import (18, 24). The wide range of MPC activity values may be attributed to several factors. First, the source of the isolated mitochondria being assayed, species and tissues, could have unique characteristics that contribute to the variability. Second, the temperatures at which the assays were performed, from room temperature down to 4 °C, directly affect MPC specific activity. Third, the source of protons required for co-transport could also contribute to differences in observed MPC K_m and V_{max} values. For example, the driving force provided by ascorbate/TMPD is dependent on the integrity of the electron transport chain and is limited to mitochondrion-intrinsic generation of a proton-motive force. Furthermore, temperature also affects the rate of electron transfer from Complex IV to O_2 and thus generation of a proton-motive force. In contrast, generating a differential pH by diluting mitochondria into an experimental buffer system of a lower pH, as was done here, saturates the pool of protons available for co-transport with pyruvate independently of temperature. Finally, K_m and V_{max} values are calculated from initial rates, which are corrected for the amount of total mitochondrial protein used in the assays. The absolute amount of MPC protein will vary depending upon the mitochondrial source and the conditions being examined. Furthermore, investigation of MPC activity in intact mitochondrial preparations required normalization to mitochondrial protein content. Given the multitude of experimental approaches, it is not surprising to see variance in reported K_m and V_{max} values.

The most direct comparison with our present results can be made to a study that was conducted at a similar temperature and utilized a pH gradient to drive uptake (18). This previous study, using isolated rat liver mitochondria, reported a K_m of 150 ± 20 μM, which is ~5.4- and ~2.1-fold less specific than the K_m values we measured here for mouse and rat liver mitochondria, respectively. Furthermore, this previous report determined a V_{max} of 0.54 ± 0.03 nmol/min/mg of mitochondrial protein, which is ~2-fold slower for mouse and ~2.6-fold slower for rat compared with our calculated values. The differences observed between mouse and rat liver MPC activity may reflect the comparatively greater basal metabolic rate of the mouse.

Pyruvate uptake directly measures the transport of pyruvate across the mitochondrial inner membrane by the activity of the MPC. Although MPC activity is required for mitochondrial

TABLE 1
Reported K_m and V_{max} values for the MPC
RT, room temperature.

Tissue of origin	Proton-motive force	Temperature	K_m	V_{max}	Sample size	Ref.
		°C	μM	nmol/min/mg		
Rat heart (young)	Ascorbate/TMPD	10	210 ± 15	6.8 ± 0.7	$n = 5$ experiments	25
Rat heart (old)	Ascorbate/TMPD	10	222 ± 23	4.2 ± 0.5	$n = 5$ experiments	25
Rat liver	ΔpH	6	150 ± 20	0.54 ± 0.03	$n = 15$ observations	18
Rat liver (control)	Ascorbate/TMPD	RT	840 ± 90	43.1 ± 3.8	$n = 4$ experiments	26
Rat liver (glucagon)	Ascorbate/TMPD	RT	1170 ± 130	74.83 ± 1.99	$n = 4$ experiments	26
Rat liver	Ascorbate/TMPD	RT		27.52 ± 1.55	$n = 19$ experiments	27
Rat liver	Passive uptake	20	640 ± 10	19.8 ± 0.5	$n = 4–6$	28
Ehrlich ascites	Passive uptake	20	643 ± 20	11.8 ± 0.6	$n = 4–6$	28
Morris 44 hepatoma	Passive uptake	20	740 ± 30	11.6 ± 0.8	$n = 4–6$	28
Morris 3924A hepatoma	Passive uptake	20	1100 ± 70	4.7 ± 0.5	$n = 4–6$	28
Mouse liver	ΔpH	4	28.0 ± 3.9	1.08 ± 0.05	$n = 3–10$ (per concentration)	This report
Mouse liver (valinomycin)	ΔpH	4	20.3 ± 7	0.75 ± 0.08	$n = 4–9$ (per concentration)	This report
Rat liver	ΔpH	4	71.2 ± 17	1.42 ± 0.14	$n = 4$ (per concentration)	This report

pyruvate oxidation, these processes are not always coupled 1:1. Upon MPC-dependent uptake, pyruvate can be carboxylated to oxaloacetate by pyruvate carboxylase, oxidized to acetyl-CoA by the pyruvate dehydrogenase complex, or transaminated to alanine by alanine aminotransferase 2. Monitoring pyruvate oxidation effectively observes the activity of the pyruvate dehydrogenase complex wherein NADH is produced and then oxidized by Complex I for electron transport. As such, pyruvate oxidation only observes one branch of intramitochondrial pyruvate metabolism and is not coupled to relative MPC activity. As shown above, MPC specific activity was not different between the fed and fasted liver mitochondria when measured by radiolabeled pyruvate uptake assays. However, significant differences were observed when pyruvate oxidation was assessed in the same mitochondrial preparations. This illustrates the importance of measuring the MPC specific activity directly as a distinct biochemical parameter rather than relying upon pyruvate oxidation as a surrogate measurement.

We expect our assay will be complementary to developing technologies for measuring metabolite flux in living cells. Recently, MPC1 and MPC2 constructs were genetically encoded with C-terminal tags that together form a bioluminescent resonance energy transfer system. Conformational changes in the MPC when transporting pyruvate bring the C-terminal tags into close proximity, allowing for specific emission of light from the excited fluorophore (6). Importantly, MPC flux *in vivo* is a compound parameter that is affected by the MPC specific activity, intramitochondrial pyruvate metabolism, and cellular pyruvate metabolism. Thus, measurements of MPC flux do not resolve the MPC specific biochemical activity. Accordingly, the radiolabeled pyruvate uptake assay persists as a fundamental assay to observe the kinetics of the MPC specific activity.

The focus of this report has been to describe a novel method for measuring pyruvate uptake by mitochondria isolated from animal liver. We expect this method will be useful for additional applications because the material and pore size of the filters can be changed to be compatible with other kinds of samples. As an example, we expect it could be adapted for measurements of MPC activity in permeabilized, cultured cells after testing for filter combinations that retain sample but are not clogged. Furthermore, we expect the scalability of our method could enable mitochondria isolated from cultured cells and liposomes reconstituted with purified transporter to be assayed in a similar manner. Finally, we propose that this method will be useful for measuring mitochondrial uptake of metabolites beyond pyruvate where a radiolabeled form and a chemical inhibitor are available.

In conclusion, we illustrate a 96-well scaled method to assay MPC-dependent pyruvate uptake into isolated mitochondria. Smaller sample requirements coupled to multiplexed processing markedly increased throughput compared with previously reported methods. We applied this method to measure and provide the first report on the K_m and V_{max} of the mouse liver MPC activity. We expect this method will be of value for understanding the contribution of the MPC activity to health and disease states where pyruvate metabolism is expected to play a prominent role.

Author Contributions—L. R. G., A. J. R., and E. B. T. designed the assays, analyzed the results, and wrote the manuscript.

Acknowledgments—We thank Brett Wagner and the Radiation and Free Radical Research Facility for help running the experiments utilizing the Seahorse Bioscience XF96 analyzer. We also thank the University of Iowa's Creative Media Group and the photography services of Susan McCellen, who produced the photographs utilized in Fig. 2.

References

1. Bricker, D. K., Taylor, E. B., Schell, J. C., Orsak, T., Boutron, A., Chen, Y. C., Cox, J. E., Cardon, C. M., Van Vranken, J. G., Dephoure, N., Redin, C., Boudina, S., Gygi, S. P., Brivet, M., Thummel, C. S., and Rutter, J. (2012) A mitochondrial pyruvate carrier required for pyruvate uptake in yeast, *Drosophila*, and humans. *Science* **337,** 96–100
2. Herzig, S., Raemy, E., Montessuit, S., Veuthey, J. L., Zamboni, N., Westermann, B., Kunji, E. R., and Martinou, J. C. (2012) Identification and functional expression of the mitochondrial pyruvate carrier. *Science* **337,** 93–96
3. Gray, L. R., Tompkins, S. C., and Taylor, E. B. (2014) Regulation of pyruvate metabolism and human disease. *Cell. Mol. Life Sci.* **71,** 2577–2604
4. Saudek, V. (2012) Cystinosin, MPDU1, SWEETs and KDELR belong to a well-defined protein family with putative function of cargo receptors involved in vesicle trafficking. *PLoS One* **7,** e30876
5. Bender, T., Pena, G., and Martinou, J. C. (2015) Regulation of mitochondrial pyruvate uptake by alternative pyruvate carrier complexes. *EMBO J.* **34,** 911–924
6. Compan, V., Pierredon, S., Vanderperre, B., Krznar, P., Marchiq, I., Zamboni, N., Pouyssegur, J., and Martinou, J. C. (2015) Monitoring mitochondrial pyruvate carrier activity in real time using a BRET-based biosensor:

investigation of the Warburg effect. *Mol. Cell* **59,** 491–501
7. Gray, L. R., Sultana, M. R., Rauckhorst, A. J., Oonthonpan, L., Tompkins, S. C., Sharma, A., Fu, X., Miao, R., Pewa, A. D., Brown, K. S., Lane, E. E., Dohlman, A., Zepeda-Orozco, D., Xie, J., Rutter, J., Norris, A. W., Cox, J. E., Burgess, S. C., Potthoff, M. J., and Taylor, E. B. (2015) Hepatic mitochondrial pyruvate carrier 1 is required for efficient regulation of gluconeogenesis and whole-body glucose homeostasis. *Cell Metab.* **22,** 669–681
8. McCommis, K. S., Chen, Z., Fu, X., McDonald, W. G., Colca, J. R., Kletzien, R. F., Burgess, S. C., and Finck, B. N. (2015) Loss of mitochondrial pyruvate carrier 2 in the liver leads to defects in gluconeogenesis and compensation via pyruvate-alanine cycling. *Cell Metab.* **22,** 682–694
9. Schell, J. C., Olson, K. A., Jiang, L., Hawkins, A. J., Van Vranken, J. G., Xie, J., Egnatchik, R. A., Earl, E. G., DeBerardinis, R. J., and Rutter, J. (2014) A role for the mitochondrial pyruvate carrier as a repressor of the Warburg effect and colon cancer cell growth. *Mol. Cell* **56,** 400–413
10. Vacanti, N. M., Divakaruni, A. S., Green, C. R., Parker, S. J., Henry, R. R., Ciaraldi, T. P., Murphy, A. N., and Metallo, C. M. (2014) Regulation of substrate utilization by the mitochondrial pyruvate carrier. *Mol. Cell* **56,** 425–435
11. Yang, C., Ko, B., Hensley, C. T., Jiang, L., Wasti, A. T., Kim, J., Sudderth, J., Calvaruso, M. A., Lumata, L., Mitsche, M., Rutter, J., Merritt, M. E., and DeBerardinis, R. J. (2014) Glutamine oxidation maintains the TCA cycle and cell survival during impaired mitochondrial pyruvate transport. *Mol. Cell* **56,** 414–424
12. Zhang, F., Xu, X., Zhou, B., He, Z., and Zhai, Q. (2011) Gene expression profile change and associated physiological and pathological effects in mouse liver induced by fasting and refeeding. *PLoS One* **6,** e27553
13. Zhang, F., Xu, X., Zhang, Y., Zhou, B., He, Z., and Zhai, Q. (2013) Gene expression profile analysis of type 2 diabetic mouse liver. *PLoS One* **8,** e57766
14. Zahlten, R. N., Hochberg, A. A., Stratman, F. W., and Lardy, H. A. (1972) Pyruvate uptake in rat liver mitochondria: transport or adsorption? *FEBS Lett.* **21,** 11–13
15. Halestrap, A. P., and Denton, R. M. (1974) Specific inhibition of pyruvate transport in rat liver mitochondria and human erythrocytes by α-cyano-4-hydroxycinnamate. *Biochem. J.* **138,** 313–316
16. Aires, C. C., Soveral, G., Luís, P. B., ten Brink, H. J., de Almeida, I. T., Duran, M., Wanders, R. J., and Silva, M. F. (2008) Pyruvate uptake is inhibited by valproic acid and metabolites in mitochondrial membranes. *FEBS Lett.* **582,** 3359–3366
17. Angaman, D. M., Petrizzo, R., Hernández-Gras, F., Romero-Segura, C., Pateraki, I., Busquets, M., and Boronat, A. (2012) Precursor uptake assays and metabolic analyses in isolated tomato fruit chromoplasts. *Plant Methods* **8,** 1
18. Halestrap, A. P. (1975) The mitochondrial pyruvate carrier. Kinetics and specificity for substrates and inhibitors. *Biochem. J.* **148,** 85–96
19. Rogers, G. W., Brand, M. D., Petrosyan, S., Ashok, D., Elorza, A. A., Ferrick, D. A., and Murphy, A. N. (2011) High throughput microplate respiratory measurements using minimal quantities of isolated mitochondria. *PLoS One* **6,** e21746
20. Bradford, M. M. (1976) A rapid and sensitive method for the quantitation of microgram quantities of protein utilizing the principle of protein-dye binding. *Anal. Biochem.* **72,** 248–254
21. Fernández-Vizarra, E., López-Pérez, M. J., and Enriquez, J. A. (2002) Isolation of biogenetically competent mitochondria from mammalian tissues and cultured cells. *Methods* **26,** 292–297
22. Fernández-Vizarra, E., Ferrín, G., Pérez-Martos, A., Fernández-Silva, P., Zeviani, M., and Enríquez, J. A. (2010) Isolation of mitochondria for biogenetical studies: an update. *Mitochondrion* **10,** 253–262
23. Gogvadze, V., Orrenius, S., and Zhivotovsky, B. (2006) Multiple pathways of cytochrome c release from mitochondria in apoptosis. *Biochim. Biophys. Acta* **1757,** 639–647
24. Papa, S., Francavilla, A., Paradies, G., and Meduri, B. (1971) The transport of pyruvate in rat liver mitochondria. *FEBS Lett.* **12,** 285–288
25. Paradies, G., and Ruggiero, F. M. (1990) Age-related changes in the activity of the pyruvate carrier and in the lipid composition in rat-heart mitochondria. *Biochim. Biophys. Acta* **1016,** 207–212
26. Titheradge, M. A., and Coore, H. G. (1976) The mitochondrial pyruvate carrier, its exchange properties and its regulation by glucagon. *FEBS Lett.* **63,** 45–50
27. Titheradge, M. A., and Coore, H. G. (1975) Initial rates of pyruvate transport in mitochondria determined by an "inhibitor-stop" technique. *Biochem. J.* **150,** 553–556
28. Paradies, G., Capuano, F., Palombini, G., Galeotti, T., and Papa, S. (1983) Transport of pyruvate in mitochondria from different tumor cells. *Cancer Res.* **43,** 5068–5071